Behavioral/Systems/Cognitive

Multiple Arithmetic Operations in a Single Neuron: The Recruitment of Adaptation Processes in the Cricket Auditory Pathway Depends on Sensory Context

K. Jannis Hildebrandt,[1] Jan Benda,[2] and R. Matthias Hennig[1]

[1]Department of Biology, Humboldt-Universität zu Berlin, 10115 Berlin, Germany, and [2]Department Biology II, Ludwig-Maximilians-Universität, 82152 Munich, Germany

Sensory pathways process behaviorally relevant signals in various contexts and therefore have to adapt to differing background conditions. Depending on changes in signal statistics, this adjustment might be a combination of two fundamental computational operations: subtractive adaptation shifting a neuron's threshold and divisive gain control scaling its sensitivity. The cricket auditory system has to deal with highly stereotyped conspecific songs at low carrier frequencies, and likely much more variable predator signals at high frequencies. We proposed that due to the differences between the two signal classes, the operation that is implemented by adaptation depends on the carrier frequency. We aimed to identify the biophysical basis underlying the basic computational operations of subtraction and division.

We performed *in vivo* intracellular and extracellular recordings in a first-order auditory interneuron (AN2) that is active in both mate recognition and predator avoidance. We demonstrated subtractive shifts at the carrier frequency of conspecific songs and division at the predator-like carrier frequency. Combined application of current injection and acoustic stimuli for each cell allowed us to demonstrate the subtractive effect of cell-intrinsic adaptation currents. Pharmacological manipulation enabled us to demonstrate that presynaptic inhibition is most likely the source of divisive gain control.

We showed that adjustment to the sensory context can depend on the class of signals that are relevant to the animal. We further revealed that presynaptic inhibition is a simple mechanism for divisive operations. Unlike other proposed mechanisms, it is widely available in the sensory periphery of both vertebrates and invertebrates.

Introduction

Sensory neurons need to transform a wide range of stimuli while using a limited signaling range. One solution to this problem is that this transformation—as reflected in the neuron's response curve—changes with the sensory context. Essentially, such adaptive operations on the response curve result from computations between a given signal and its background and can largely be classified into two types: subtractive and divisive (Silver, 2010; Fig. 1*A*). Subtraction shifts the threshold of the response curve while the slope remains unchanged and high resolution for small differences in the input is retained. Division, also referred to as gain control, alters the slope of the curve and extends the dynamic output range. These elementary mathematical computations constitute building blocks for both the CNS (Carandini and Heeger, 1994; Peña and Konishi, 2001) and optimal encoding of stimuli in early sensory processing across modalities and species (Barlow and Levick, 1965, Laughlin, 1994; Carandini and Heeger, 1994; Harris et al., 2000; VanLeeuwen et al., 2009; Wen et al., 2009). While the biophysical machinery behind subtractive changes on the level of single cells is well documented (Holt and Koch, 1997; Chance et al., 2002; Gabbiani et al., 2002; Benda and Herz, 2003), most mechanisms proposed to mediate divisive gain control demand a large synaptic background not available in the sensory periphery (Abbott et al., 1997; Chance et al., 2002; Gabbiani et al., 2002; Baca et al., 2008; Rothman et al., 2009).

One role for adaptation in the periphery may be to ensure reliable coding for a specific class of signals rather than all available sensory input. If so, the recruited mechanisms implementing mathematical operations may depend on the signal class predominantly processed: subtraction if the primary change in the signal is mean intensity, and division if the variance of signal's intensity is altered (Brenner et al., 2000). Here, we aimed to examine the context-specificity of the modulatory changes on the input response curve of a single, first-order auditory interneuron in crickets (AN2) involved in the processing of two very different classes of signals. At low sound frequencies (~3 kHz), the AN2 is mainly devoted to processing the temporal structure of conspecific songs. These are highly stereotyped signals that probably vary mostly in their mean intensity and thus could primarily demand subtractive adjustment of the response curve for distance invariant representation (Benda and Hennig, 2008). How-

Received May 23, 2011; revised July 25, 2011; accepted July 26, 2011.

Author contributions: K.J.H., J.B., and R.M.H. designed research; K.J.H. performed research; K.J.H. analyzed data; K.J.H. wrote the paper.

The work presented here was funded by the German Research Foundation (DFG, Collaborative Research Centre 618). We thank Lucy Anderson for comments on a previous version of this manuscript.

Correspondence should be addressed to K. Jannis Hildebrandt at his present address: Ear Institute, University College London, London, WC1X 8EE, UK. E-mail: j.hildebrandt@ucl.ac.uk.

DOI:10.1523/JNEUROSCI.2556-11.2011

 0270-6474/11/3114142-09$15.00/0

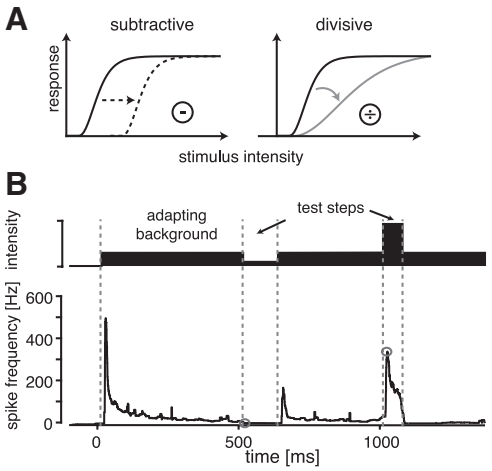

Figure 1. Evaluation of response curves. ***A***, Two effects of adaptation on response curves as discussed in the present work: subtraction (left) shifts the responses along the input axis, while division (right) scales the slope of the curve. Note that both operations act on the input axis of the response curve, thereby preserving the range of response values available for coding. Another possibility would be divisive scaling of the response axis, which alters the slope but also causes a decrease of the maximal response. Here, we only consider operations on the input axis, pictured in ***A***. ***B***, Stimulation paradigm. To construct onset-response curves at specific adaptation levels, a background stimulus was presented and short, rectangular steps of the stimulus amplitude introduced (***B***, upper trace). These test steps were gated with 2 ms rise and fall times (not visible at this scale). The background stimulus was long enough to fully adapt to this stimulus. Neural responses for each test intensity were quantified as the spike-frequency responses at the beginning of the test pulses, indicated by the gray circles in ***B***. Spike frequency was quantified as the mean of the inverse of the interspike intervals in all trials, separately for each time step (resolution 1 ms). The onset-response curve was constructed from these responses as a function of the intensity of the corresponding test stimuli.

ever, at higher frequencies (>15 kHz), crickets mainly detect echolocation sounds of preying bats (Moiseff et al., 1978), a signal class that is likely to be much more diverse in both variance and mean of the intensity, possibly requiring both subtractive and divisive adaptation.

We tested the hypothesis that sensory context determines the mathematical operations that are implemented by adaptation. First, we tested how adaptation changes the input response functions in two behaviorally relevant frequency ranges in a single auditory interneuron. In a second step, we aimed to show which mechanisms are responsible for the different operations and how context-dependent recruitment of these is achieved.

Materials and Methods

Animals and preparation

Female crickets of the species *Teleogryllus leo* were used. For preparation, both pairs of wings and the mesothoracic and metathoracic legs were removed. The animal was fixed ventral side up to a small platform and the prothoracic legs with the ears were waxed to pins at the coxae and the tarsi in a normal walking position. For extracellular recordings, ascending and descending connectives from the prothoracic ganglion were cut to reduce neuronal background activity. For intracellular recordings and pharmacological interventions, the prothoracic ganglion was exposed and stabilized by a small metal platform. Data presented here resulted from 30 preparations.

Electrophysiology

Extracellular recording. Two extracellular hook electrodes were made from tungsten wire and placed in parallel around one of the two connectives ascending from the prothoracic ganglion. These connectives contain the axon of the ascending interneuron AN2. Vaseline was placed around connectives and hooks to isolate the electrodes electrically and keep the connective from drying out. The voltage trace was amplified differentially (npi, EXT-10C) and bandpass-filtered with cutoff frequencies of 300 Hz and 3 kHz (npi, DPA 2F). The trace was then digitized at 20 kHz sampling rate (National Instruments, PCI-6014) and stored to the hard disk of a personal computer. Spikes of the AN2 were detected on the basis of the amplitude peaks of the voltage trace using custom software (MATLAB, The MathWorks). We recorded from 20 animals extracellularly.

Intracellular recordings. Intracellular recordings were obtained with sharp electrodes pulled on a horizontal puller (P87, Sutter Instruments) using borosilicate glass (GCF100F10, Harvard Apparatus). Electrode tips were filled with a 3.5% solution of Lucifer yellow (Sigma-Aldrich) in 0.5 M LiCl. Electrodes had resistances of 40–60 MΩ, allowing for the large currents necessary in our experiments to pass through. The AN2 was recorded medially in the prothoracic ganglion in the neuropile from which the ascending axons originates (Wohlers and Huber, 1978). The voltage was amplified (SEC05LX, npi electronic), and subsequently it was digitized and stored as described for the extracellular recordings. After completion of experiments, the prothoracic ganglion was removed, fixed in 4% paraformaldehyde, dehydrated, and cleared in methylsalicylate. The stained cells were identified under a fluorescent microscope according to their characteristic morphology. Intracellular recordings presented here were obtained from 10 different animals. From the digitized recordings, the spike times were extracted by a peak detection algorithm (Todd and Andrews, 1999).

Application of picrotoxin

For the experiments with picrotoxin, the prothoracic ganglion was exposed and a glass electrode with a broken tip was used to perforate the membrane of the ganglion 5–7 times. This was done during extracellular recordings only. Following the control stimulus protocol, Ringer's solution was taken off and picrotoxin dissolved in Ringer's solution was applied. For the next 15 min, Ringer's solution with picrotoxin was replaced every minute and afterward, the stimulus protocol was tested again. For the wash condition, the picrotoxin Ringer's solution was replaced and during a 15 min period the ganglion was rinsed every minute with fresh Ringer's solution. For another 20 min, Ringer's solution was replaced every 5 min. After this procedure, the stimulus ensemble was presented again. Only preparations, in which the recordings lasted for the long time of this procedure (~100 min) were used for the analysis (six animals).

Stimulation

Acoustic stimuli. Acoustic stimuli were delivered via one of two speakers (D28/2, Dynaudio) located in a angle 35 cm away from the animal, placed in a cage lined with sound absorbing foam. Signals were delivered by custom-made software (LabView, National Instruments) via 100 kHz D/A-converter (PCI-6014, National Instruments), attenuated under digital control (PA5, Tucker-Davis Technologies), and amplified (GTA 2100B, Blaupunkt). Sound intensities were calibrated with a 1/2 inch microphone (type 2209, Brüel and Kjær).

Current stimuli. Current stimuli were digitally stored and delivered by custom-made software (LabView) via the recording electrode. The amplifier (SEC05LX, npi electronic) was set to discontinuous current-clamp mode. Discontinuous switching rates were adjusted on a cell-to-cell basis to values of 15–20 kHz.

Stimulus protocols. In all experiments, response curves were obtained by presenting short test stimuli with rise and fall times of 2 ms of either 50 or 100 ms duration. For acoustic stimuli, these test stimuli represent rectangular amplitude modulation of one of the two carrier frequencies. For the current stimuli, they constitute ramped steps of the amplitude of the current. To obtain the adapted response curves, these pulses were preceded by at least 500 ms of the adapting background (Fig. 1*B*). If the amplitude of the test stimulus was lower than that of the adaptor, 100 ms test stimuli were used; otherwise, 50 ms stimuli were used. When adaptor and test stimulus were both acoustic and of the same frequency, 2 ms ramps led linearly from the adapting background to the test amplitude. For current and cross-frequency adaptation experiments, we obtained the latency for each stimulation mode separately and corrected the onset in such a way that switching off the adaptor and switching on of the test

stimulus coincided. Latency for current stimuli was shortest (2.4 ± 0.7 ms), followed by the high-frequency (9.7 ± 2.7 ms) and low-frequency (12.4 ± 3.1 ms) stimuli. All stimuli were repeated at least 15 times.

Data analysis

Spike frequency $f(t)$ was estimated by taking the inverse of the interspike interval (ISI) between the preceding and the following spike at each time t for each test stimulus and all trials separately at a resolution of 1 kHz. At the time of a spike, we used the value of the preceding ISI. For all times before the first and after the last spike during the test stimulus, we set $f(t)$ to zero. The mean spike frequency and SD were obtained by averaging across trials for each test stimulus separately. At very low spike frequencies, the precision of this measure is restricted by the duration of the test pulse. Even if true spike frequency was >0, we may not have been able to detect this if ISIs became larger than half of the duration of the evaluation window, since $f(t)$ was set zero if <2 spikes occurred in the window. This is most relevant for test stimuli smaller than the background (duration 100 ms), and in these cases, we would have underestimated spike frequencies <20 Hz. However, almost all of the suprathreshold response curve of the AN2 were far above 20 Hz as can be seen for the unadapted curves, which were measured using 500 ms test stimuli (for more details, see Hildebrandt et al., 2009).

The onset response was obtained by taking the maximum of the mean spike frequency during the first 30 ms after stimulus onset. All error bars reflect the standard deviation (SD) of the spike frequency at the maximum spike frequency across trials.

For the parameterization of the unadapted response curves, a squared hyperbolic tangent of the form

$$f_{on}(I) = \begin{cases} f_{max}\tanh^2(k(I_{th} - I)) & ; \text{if } I > I_{th} \\ 0 & ; \text{else} \end{cases},$$

was used. Squaring was introduced to match the asymmetric shape of the response curves. I is the input intensity in dB, I_{th} is the threshold of the neuron, and f_{max} is the maximal spike frequency of the response curve. k is a slope factor and can be used to calculate the slope at the turning point of the curves:

$$S_{on} = \frac{4}{3\sqrt{3}} f_{max} k.$$

For the quantifications of shift and slope change, the adapted onset-response curves were parameterized using the same value of f_{max} as for the unadapted curve. Only k and I_{th} were fit to the data.

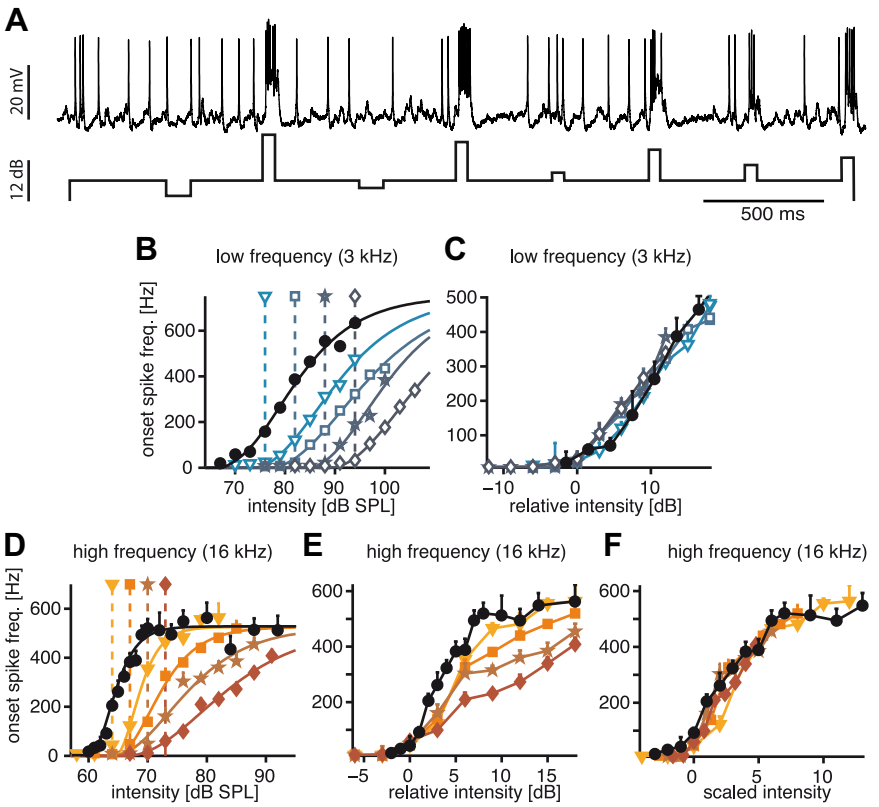

Figure 2. Effect of adaptation on onset-response curves at two different carrier frequencies. ***A***, Example voltage trace of an AN2 response to the adaptation paradigm (see Fig. 1). The stimulus envelope of the amplitude modulation of an acoustic stimulus is displayed below. Both intensities above and below the adapting background were presented to obtain the full response curves. ***B***, Example of response curves of an AN2 after adaptation to different background intensities at a carrier frequency of 3 kHz. The black dots and lines represent the onset-response curves without adaptation. Colored lines and symbols depict onset-response curves after adaptation to the background intensity indicated by the respective symbols above the graph. The onset-response curves were evaluated at the onset of the amplitude steps in the bottom of ***A***. ***C***, Same data as ***B***, but with the intensity relative to the respective adapting background for each adapted response curve (adapter level was set to 0 dB). ***D***, ***E***, Adapted response curves for a carrier frequency of 16 kHz, for explanation see (***B***, ***C***). ***F***, Since subtracting the background did not eliminate all of the adaptation effects at 16 kHz (***D***), the input intensity was additionally divided by the adaptation background to show the divisive effect of adaptation. Error bars indicate SD, solid lines in ***B*** and ***D*** stem from hyperbolic tangent fits to the data. The color scheme used here (open blue for low-frequency stimulation, closed red/orange for high-frequency stimulation) is consistently used in all subsequent figures.

Results

Changes of the response curves in the two frequency channels

The AN2 of crickets is sensitive in two frequency ranges that correspond to two different behavioral contexts, mate selection and predator avoidance (Moiseff et al., 1978). It receives direct input from two populations of receptor neurons (Hennig, 1988) that are sensitive to two separate frequency ranges (Imaizumi and Pollack, 1999). Since the requirements on coding and processing in these two contexts also differ (Marsat and Pollack, 2004), we first tested whether adaptation changes the response curve of the AN2 in a frequency-specific way. We presented test stimuli of different intensities with either no adapting background (unadapted response curve) or preceded by a defined adaptation level of the same carrier frequency (Figs. 1*B*, 2*A*). Both carrier frequencies were tested separately in this way, and the onset response to each test step was quantified by the instantaneous spike frequency.

Examples of single cells are shown in Figure 2. Response curves in the low-frequency channel retained their overall shape, but thresholds shifted considerably depending on the adaptation level. This shift was observed over a wide range of intensities, in some cases up to 20 dB (Fig. 2*B*). When the adapting background was subtracted from the absolute stimulation level, all adapted curves matched the unadapted curve, demonstrating a strictly subtractive effect of the adapting background intensity at the low carrier frequency (Fig. 2*C*). At the high carrier frequency, response curves were shifted as at low frequencies, but also showed a clear decrease of the slope in response to different adapting backgrounds (Fig. 2*D*). Plotting relative rather than absolute intensities revealed this change to be subtractive (Fig. 2*E*); however, adaptation also induced a change of the slope of the response curves (Fig. 2*E*). In a second step, we divided the input intensities

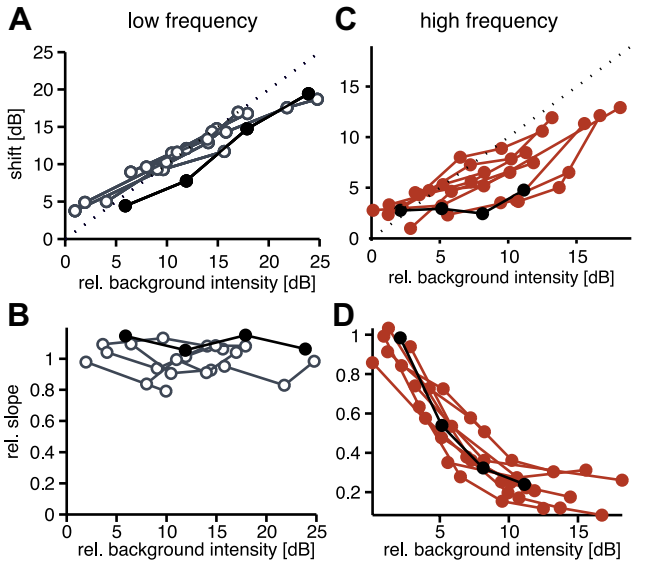

Figure 3. Changes of onset-response curves for all recorded cells. ***A***, Summary of shift of the threshold as a function of the adapting background for the low-frequency carrier (3 kHz). The values for the shift were derived from hyperbolic tangent fits to the adapted response curves (see Fig. 2*B*). Each data point represents one tested background intensity; points connected by lines were recorded in the same cell. The black symbols represent the cell displayed in Figure 2*B*. Background intensities are plotted relative to the unadapted threshold for each cell. The shift was quantified by the difference in threshold between the adapted and the unadapted response curve. The dashed line has a slope of 1, representing a shift of the threshold exactly to the background level. Curves below the diagonal come from cells that exhibited only a small shift of threshold. ***B***, Summary of slope changes due to adaptation for a 3 kHz carrier derived from hyperbolic fits to the adapted response curves. The slope is given relative to the respective unadapted curve—values below 1 indicate shallower response curves than the unadapted curve. ***C***, ***D***, Summary of data recorded at 16 kHz, plotted in the same way as ***A*** and ***B***, respectively.

of the adapted response curves by the respective relative background intensities corrected by a single constant scaling factor (Fig. 2*F*). These input-divided curves all matched the original, unadapted curve very well, demonstrating that adaptation at high carrier frequencies has both a subtractive and divisive effect on the input dimension of the response curves. For those cells that were recorded intracellularly, we performed the same analysis for the voltage input instead of the spike output. This analysis yielded the same results (data not shown).

To fully quantify this effect for all recorded cells, we analyzed the change of two parameters of the fits to the adapted response curves: threshold shift and slope. If the effect was purely subtractive, a linear relation between background and threshold shift is expected and the slope should remain constant. The prediction for a divisive gain control is a monotonically decreasing relationship between the background intensity and the slope of the respective curve. For both carrier frequencies, a positive linear relation between background and threshold shift was observed (Fig. 3*A*,*C*). For the low frequency, background and threshold shift were highly correlated, if all data points in Figure 3*A* were taken into account ($r = 0.95$, $p < 0.0001$). This correlation can also be observed, if it is calculated for individual cells separately (mean $r = 0.99$, $p < 0.05$, including all cells for which more than two adapted response curves were measured). In the range between 0 and 20 dB of relative background, the slope of the linear relation was 1, indicating that the threshold shifted exactly to the background intensity (Fig. 3*A*). At the high frequency, the shift was frequently below the relative background intensity (Fig. 3*C*), which indicated a smaller subtractive contribution due to adaptation, but a significant correlation at the population level was still observed ($r = 0.63$, $p < 0.001$; mean of single cells: $r = 0.91$, $p = 0.15$).

At the low frequency, no change in slope was observed for all cells tested, as predicted for strictly subtractive adaptation (Fig. 3*B*; population: $r = 0.05$, $p = 0.81$; mean of single cells: $r = 0.03$, $p = 0.59$). At the high frequency, there was a linear relationship between relative background and slope of the response curve up to 10 dB (Fig. 3*D*; population $r = 0.92$, $p < 0.0001$; mean of single cells: $r = 0.97$, $p < 0.05$). Thus, adaptation had a reliable divisive effect at the high frequency.

The role of adaptation currents within AN2

Having observed the significant difference due to adaptation in the two carrier frequency channels, we aimed to determine where in the auditory pathway the two different effects—subtractive and divisive—arise. Since AN2 receives direct input from receptor neurons, there are four potential locations: (1) the two different populations of receptor neurons for the two different carriers (Fig. 4*A*, no. 1), (2) the synaptic connections between receptor neurons and AN2 (Fig. 4*A*, no. 2), (3) direct inhibition of the AN2 itself, possibly originating from the omega neuron (Selverston et al., 1985), or finally, (4) adaptation currents within the AN2 that are activated by its own activity (Fig. 4*A*, nos. 3, 4).

First we tested the effect of adaptation currents within the AN2 itself. The protocol resembled that of the first experiment (Fig. 2), but the background adaptation was now introduced by current injection that elicited spiking only in the AN2. Test stimuli were again acoustic stimuli of the two carrier frequencies. Therefore, the adaptation mechanism activated in these experiments is shared by both frequency channels; thus, the effect of adaptation to current stimuli should be the same in each instance (Fig. 4*A*).

Adaptation within the AN2 activated by current injection had an effect in both frequency channels (Fig. 4*B*). This effect operated subtractively on the response curves at both carriers (Fig. 4*B*,*C*; low frequency: $r = 0.85$, $p < 0.001$; high frequency: $r = 0.90$, $p < 0.0001$), as predicted from modeling studies (Benda and Herz, 2003). As expected, the effect of adaptation to current injections was indistinguishable for both carriers (Fig. 4*B–D*). There was no indication of a change of slope for the response curves due to adaptation currents (Fig. 4*D*; low: $r = -0.25$, $p = 0.43$; high: $r = 0.07$, $p < 0.81$). In summary, adaptation currents within the AN2 contributed to the subtractive effect observed in both carrier frequencies (Fig. 3*A*,*C*), but cannot account for the divisive operation observed with acoustic stimulation at the high carrier frequency.

Cross-frequency adaptation between both frequency channels

Since divisive gain control is not due to adaptation within AN2 itself (Fig. 4), its origin must be located more peripherally. Three possible locations remain (Fig. 4*A*): (1) within each single receptor, (2) at the synapses either via presynaptic inhibition or by synaptic depression, or (3) postsynaptic inhibition to AN2 (e.g., from the omega neuron). If the effect of adaptation originates within either of the two receptor populations, it should not be observed if the pathway is adapted at one carrier frequency and tested at the other. Similarly, if the divisive effect is mediated by frequency-specific presynaptic inhibition, its occurrence should be restricted to the respective frequency band. To elucidate the contribution of receptors, we performed cross-frequency adaptation experiments: the pathway was adapted by playing a con-

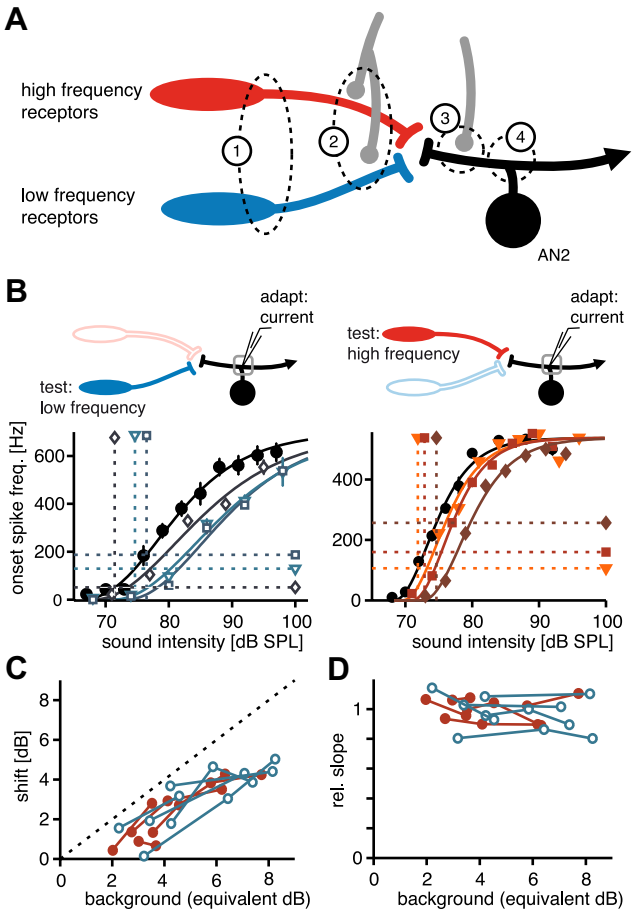

Figure 4. Activation of adaptation currents in response to current injections. In ***A***, inputs to AN2 and possible locations of adaption are shown. AN2 receives direct input from two receptor populations (low and high carrier frequency). Additionally, there are inhibitory inputs on the presynaptic terminals whose origin is unknown (gray, no. 2). AN2 also receives direct postsynaptic inhibition via another auditory interneuron, the omega neuron (gray, no. 3). Potential locations of mechanisms of adaptation as observed in AN2 during acoustic stimulation include adaptation currents in the receptor neurons (1), presynaptic inhibition (2), postsynaptic inhibition (3), and spiking-activated adaptation currents within AN2 itself (4). The gray box at the top of ***B*** shows only the adaptation mechanisms that are activated by the "background" current injection. Filled neurons indicate which part of the pathway is subsequently excited by the acoustic test pulses used to construct the onset-response curves in the bottom. Response curves in ***B*** are from two different cells (for details, see Fig. 2). The left panel shows response curves to 3 kHz test stimuli after different levels of current adaptors, and the right panel shows response curves measured at 16 kHz. Since background intensity (i.e., injected current) has not the same units as the response curves, the elicited onset spike frequency to the adapting current injections are used to indicate the background level by horizontal dashed lines (***B***). The vertical lines represent the "equivalent decibel" value, constructed by the intersection of the fit to the unadapted response curve with the horizontal line (***B***). ***C*** and ***D*** show response curve parameters for all recorded cells ($n = 5$ for each frequency); open blue symbols depict 3 kHz test stimuli, and solid red stimuli represent test stimuli with a 16 kHz carrier. For details, see Figure 3.

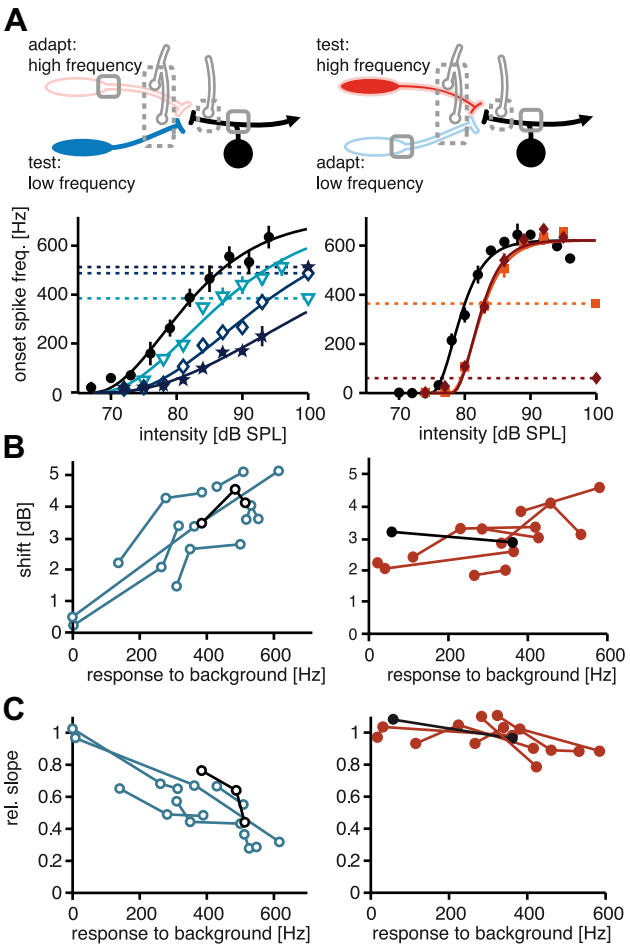

Figure 5. Cross-frequency adaptation between frequency channels. The gray boxes in the top of ***A*** illustrate the possible locations of adaptation activated by the adapting background stimulus. Dotted lines indicate locations of possible inhibitory input elicited by the background (unidentified for the presynaptic sites, omega neuron for the postsynaptic site). Filled neurons indicate which part of the pathway is subsequently excited by the acoustic test pulses used to construct the response curves in the bottom. Colors are the same as in Figure 4 (low frequency: open blue; high frequency: solid orange/red). The lower left panel of ***A*** shows an example of response curves tested at 3 kHz after adapting to a 16 kHz background (for details, see Fig. 2). The lower right panel shows response curve recorded from a different cell at 16 kHz after adapting to different levels of a 3 kHz background. Since background intensity does not have the same units as the response curves, the elicited onset response to the adapting stimuli are used to indicate the background level by horizontal dashed lines (***A***). ***B*** and ***C*** show response curve parameters for all recorded cells ($n = 7$ for each frequency); the black lines and symbols depict the respective examples shown in ***A***. For details, see Figure 4.

stant background stimulus of one carrier frequency directly followed by acoustic test pulses at the other frequency. Onset-response curves at different background levels were constructed as before (Fig. 1*B*). If the divisive effect was due to mechanisms within the high-frequency receptor population or due to synaptic depression, we would not expect a divisive effect of adaptation to high frequencies on the low-frequency response, only a shift similar to that observed in the current adaptation paradigm.

When the pathway was adapted to the low carrier frequency, the response curve to subsequent stimuli of the high carrier shifted, but did not change its slope (Fig. 5, left panels). Very low intensities near the threshold of the AN2 shown in Figure 5*A* resulted in a shift >3 dB. However, increasing the adaptation intensity of the low-frequency background further did not result in a more pronounced shift. Both effects can be observed for all seven recordings from AN2 using this stimulus paradigm (Fig. 5*B*; shift: $r = 0.61$, $p < 0.01$; slope change: $r = 0.52$, $p = 0.09$). Although the low-frequency background was able to elicit onset spike frequencies over the whole range of the response curves of AN2 (Figs. 2*A*, 5*B*,*C*), the resulting shift was usually restricted to a range between 2 and 5 dB (Fig. 5*B*). This range was in good agreement with the results shown in Figures 3*A* and 4*C*. As can be seen in Figure 3*A*, the low-frequency background never shifted the low-frequency response curves <3 dB, even at background intensities close to the threshold. Current injections, which activate the same adaptation currents within AN2 that are also elic-

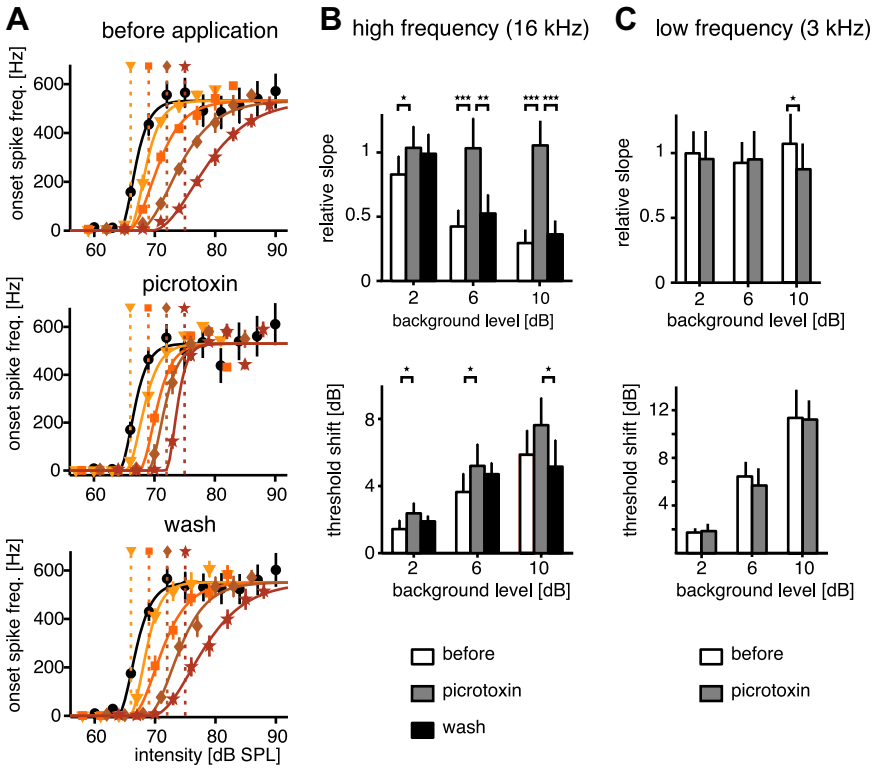

Figure 6. Change of onset-response curves due to adaptation before, during, and after the application of picrotoxin blocking GABAergic presynaptic inhibition. ***A***, Example of adapted onset-response curves for high-frequency stimulation (16 kHz) for the different conditions in a single cell (for details, see Fig. 2). ***B***, Summary of all recorded cells under the three conditions ($n = 6$). Top, Change of slope. Bottom, Threshold shift. Each cell was tested at three different adaptation levels relative to its threshold in the unadapted state in all conditions. To compare among conditions, data were parameterized as before (Fig. 3). Since the exact threshold of the unadapted neuron was evaluated only after the experiment, the background levels for the different cells were not exactly the same. Thus, to enable statistical testing, the adaptation background level—relative to the threshold—was pooled in three classes: 1–3 dB (2 dB label), 5–7 dB (6 dB), and 9–11 (10 dB). Error bars represent SD between cells. $^*p < 0.05$; $^{**}p < 0.01$; $^{***}p < 0.001$. ***C***, Same as ***B*** for the low carrier frequency.

ited in the paradigm presented here (upper panels in Figs. 4*A*, 5*A*), did not shift the response curve >5 dB (Fig. 4*C*).

We also tested how adaptation in the high-frequency channel changes response curves for low-frequency sounds (Fig. 5*A*, upper right). Here, we observed a clearly divisive effect of the high carrier frequency on the low-frequency response curves (Fig. 5, right panels). The change in slope was of a magnitude similar to the change in high-frequency response curves (Fig. 3*D*) and was seen in all seven tested cells (Fig. 5*C*, right; $r = 0.83$, $p < 0.001$). The divisive effect cannot be attributed to receptors or synaptic depression because the populations excited during adaptation and test did not overlap (Fig. 5*A*). Adaptation currents in AN2 are also excluded because the divisive effect is not seen during current injection (Fig. 4). Notably, adaptation via the high-frequency channel accomplished a divisive operation of signals in both the low- (Fig. 5*A*) and the high- (Fig. 2*C*) frequency channel.

Adaptation to high frequencies also mediated a moderate subtractive shift of low-frequency response curves (Fig. 5*B*, right; $r = 0.82$, $p < 0.001$). This shift can well be attributed to adaptation currents in AN2 as revealed by the current injection experiments (Fig. 4), since the range observed during current injection (Fig. 4*C*) is the same as that observed during cross-frequency adaptation (Fig. 5*B*, right). Other than for adaptation to low frequencies, the subtractive effect did not yield any indication of an additional inhibitory influence that would shift the response curves.

Blocking of presynaptic inhibition

The previous experiments revealed that the mechanism for divisive gain control was located neither in the receptors (Fig. 4, no. 1) nor in the AN2 itself (Fig. 4, no. 4), nor was it due to synaptic depression. Thus, inhibitory inputs remain as a source of divisive adaptation, for which there are two possible candidate sites: direct postsynaptic inhibition of the AN2 (Fig. 4, no. 3), mainly mediated by the histaminergic ω neuron that provides contralateral inhibition and improves directionality in the pathway (Watson and Hardt, 1996), and presynaptic inhibitory GABAergic terminals at the receptor axons (Fig. 4, no. 2), whose source has not yet been identified (Hardt and Watson, 1999). Presynaptic inhibition has been proposed to enable divisive gain control (Laughlin, 1994; Root et al., 2008; VanLeeuwen et al., 2009).

Taking advantage of the different transmitters, we selectively blocked GABAergic presynaptic inhibition by applying picrotoxin. We then repeated the adaptation protocol from the first experiment (Fig. 2) using high-frequency stimulation and measured adapted response curves before and during application of picrotoxin and again after washing (Fig. 6*A*). At high carrier frequencies, picrotoxin did not alter the unadapted onset-response curves, but had a profound effect on the adapted curves (Fig. 6*A*, middle panel). Without picrotoxin, the slope of the response curves changed with the adapting background. However, if picrotoxin was applied, the response curves only changed with respect to the threshold shift, and the slope remained the same, even at large background intensities. The change in slope and the threshold shift were quantified by parameterization of the response curves and were the same for the conditions with and without picrotoxin (Fig. 6*B*). For background intensities >4 dB above threshold, we observed a highly significant difference for the slope between the control condition and picrotoxin application ($p < 0.001$, Fig. 6*B*). With picrotoxin, no difference in slope between the different background adaptation levels was observed, while the comparisons between different background intensities were highly significant both before application and after washing ($p < 0.001$). Thus, picrotoxin entirely removed the divisive part of adaptation, providing strong evidence for presynaptic inhibition to mediate divisive gain control. While the divisive part was removed by picrotoxin, blocking of presynaptic inhibition induced no or only weakly significant ($p < 0.05$) differences of the subtractive threshold shift (Fig. 6*C*). For those cases in which the difference between picrotoxin and controls was significant, the threshold shift was always larger when presynaptic inhibition was blocked.

Since picrotoxin was applied to the entire ganglion, it may also affect other, not yet described, GABAergic sites in the network. To partly control for this, we also tested the effect of picrotoxin on adaptation at low carrier frequencies, at which no change of slope had been previously observed (Fig. 6*C*). If the effect of picrotoxin

on adaptation was restricted to presynaptic sites of the high-frequency pathway, no change should be seen after application of picrotoxin. Indeed, apart from a weakly significant reduction of slope at high background levels of >10 dB (Fig. 6*C*, top panel), no change was observed after application, neither for the slope nor for the threshold shift.

Discussion

The first-order interneuron AN2 in the auditory pathway of crickets receives direct synaptic input from two receptor populations (Hennig, 1988) and exhibits different forms of gain control in the two frequency channels. In the lower frequency range, a subtractive effect of the background sound was observed, while high-frequency backgrounds had a divisive effect on subsequent stimuli (Figs. 2, 3). We were able to disentangle the origins of subtractive and divisive effects by using current injection as background (Fig. 4), by performing cross-adaptation experiments (Fig. 5) and by selective blocking of presynaptic inhibition (Fig. 6). Thereby we showed that presynaptic inhibition is induced by the high-frequency channel and provides means for context-specific division of two subsequent signals along the stimulus axis (Figs. 2*E*, 3*D*).

Subtractive and divisive adaptation

Subtraction and division of inputs is an operation that forms an important part of numerous neural computations (Salinas and Thier, 2000; Silver, 2010). In sensory processing, gain control may serve to normalize contrast or variance (Brenner et al., 2000; Baccus and Meister, 2002; Dean et al., 2005) and to keep sensory neurons sensitive to broad distributions of stimuli (Olsen et al., 2008, 2010).

In the retina of both vertebrates and invertebrates, gain control has been widely described with respect to stimulus contrast (Shapley and Enroth-Cugell, 1984; Laughlin, 1989). One mechanism thought to underlie contrast normalization is a combination of logarithmic scaling and a subsequent subtractive mechanism. In the auditory field, intensity is always plotted logarithmically on a decibel scale. The cricket's receptors already encode sound linearly on this logarithmic axis (Imaizumi and Pollack, 2001), and thus a shift on the decibel scale is referred to as "subtractive" (Fig. 2). Consequently, a given signal played at different distances from the receiver varies only in the mean and not in its variance. The subtractive changes we observed at the lower frequency (Fig. 3) may thus contribute to a distance invariant representation of conspecific signals (Benda and Hennig, 2008) or to a separation of the loudest of several singing males from its background (Wimmer et al., 2008), both of which require a shift of the threshold. Where does subtractive adaptation arise? Part of it may be intrinsic adaptation within the AN2 (Fig. 4). However, the threshold shift induced by current injections that activated intrinsic mechanisms covered a smaller range than expected from acoustic adaptation at sound levels that elicited the same onset response as the current injection ("equivalent dB", Fig. 4*C*). It is likely that the subtractive effect is a combination of the adaptation currents in AN2 and adaptation mechanisms located more peripherally, either in the receptor neurons or at the synapses, a pattern that has also been reported in the auditory system of grasshoppers (Hildebrandt et al., 2009).

At higher frequencies, we observed pronounced divisive gain control (Fig. 3). At this frequency range, the most prominent role of the AN2 is predator avoidance (Moiseff and Hoy, 1978, Marsat and Pollack, 2006). At low carrier frequencies, the relevant signals are mostly stereotyped conspecific songs. However, the variance of relevant signals at high frequencies probably changes over a considerably larger range of intensities and may require a powerful divisive gain control mechanism. A second important feature of the gain control mechanism described here is that it controls input rather than output (Ayaz and Chance, 2009), thereby avoiding output saturation. It is likely that the AN2 itself includes a saturating nonlinearity, because the receptor sensitivities are distributed in crickets, resulting in a large dynamic range not of single receptors but of the entire population (Imaizumi and Pollack, 1999, 2001). Thus, in the unadapted state, the steep response curve of the AN2 reflects only the input of the part of the population with very low thresholds, because at higher intensities the AN2 is already saturated. In the context of motion-sensitive cells in the visual system of flies, it has been suggested that input control could protect postsynaptic nonlinear operations that are vulnerable to saturation (Harris et al., 2000). This is of great relevance for high-frequency processing in AN2, which has been shown to use a strongly nonlinear mechanism for predator detection (Marsat and Pollack, 2006).

In contrast to our data, onset-response curves of the AN2 in the high frequency range in *Teleogryllus oceanicus* were described to rise continuously over a large range of intensities up to 100 dB without saturation (Nolen and Hoy, 1987). However, we averaged over all cells with correction for absolute threshold. Without this correction, the mean response curve from our data also does not saturate up to 100 dB. Nevertheless, all cells recorded here displayed steep, saturating response curves on the single-cell level.

What is the source of the presynaptic inhibition?

GABAergic presynaptic terminals have been observed at cricket auditory receptor terminals (Hardt and Watson, 1999), but their origin remains elusive to date. Feedback from the brain can be discarded, because in all recordings the connectives between thorax and head were cut. The best-described inhibitory auditory interneuron in the prothorax of crickets is the omega neuron (Selverston et al., 1985; Marsat and Pollack, 2005), but it is histaminergic (Watson and Hardt, 1996). In other cricket species, two-tone experiments combining low- and high-frequency carriers revealed inhibition elicited by low-frequency sound on high-frequency stimuli (Nolen and Hoy, 1986, 1987; Libersat et al., 1994). The source of this inhibition is unknown, but its target is postsynaptic and not presynaptic to AN2.

The action of presynaptic inhibition does not seem to be very fast, since blocking did not influence the onset responses (Fig. 6*A*), indicating a polysynaptic connection with a larger latency than direct excitation. A similar indirect afferent to afferent connection via local interneurons has been described for locust wing proprioceptors (Burrows and Matheson, 1994) and wind-sensitive afferents (Boyan, 1988).

Although the source of presynaptic inhibition as observed here remains unknown, one prediction regarding the properties of a potential input to the receptor terminals can be made. The divisive effect operated over a range much larger than the dynamic range of the AN2, and thus, any potential source of presynaptic inhibition should have a response curve with a shallow slope. Notably, the response curve should not adapt in a similar manner as the AN2 or the other ascending interneuron (AN1, Benda and Hennig, 2008) to reliably inhibit according to the absolute level of the "background." In general, for every mechanism that changes response curves relative to some absolute mean or overall variance of the stimulus statistics, these absolute

values are saved in the state of adaptation of the mechanism, e.g., the state of channels mediating adaptation currents or as in the present study, in the input driving presynaptic inhibition.

Presynaptic inhibition and gain control in other systems

The term gain control has been widely used in two different contexts. The first applies mainly to control of motor activity in invertebrates (Clarac and Cattaert, 1996) and vertebrates (Rudomin, 2009) and focuses on the mechanism of presynaptic inhibition, allowing control of synaptic efficacy independent of the activity of the target synapse. The second usage of the term is in its computational meaning, a divisive operation on the response function of a neuron (Abbott et al., 1997; Chance et al., 2002; Prescott and Koninck, 2003).

While postsynaptic inhibition has been shown to act subtractively (Holt and Koch, 1997), recent evidence suggests that presynaptic inhibition provides a mechanism for a division of inputs (Root et al., 2008). GABAergic inputs to presynaptic terminals are omnipresent both in invertebrate (Clarac and Cattaert, 1996) and vertebrate (Rudomin, 2009) nervous systems. Among other effects, presynaptic inhibition mediated by $GABA_A$ has a shunting effect on the afferent terminals (Cattaert and El Manira, 1999), and acts divisively on changes of the membrane potential (Carandini and Heeger, 1994; Nelson, 1994). Thus, different levels of inhibition in response to the respective adapting background may reduce the amplitude of action potentials effective at the synaptic terminals in a divisive way, which could be reflected in postsynaptic potential amplitudes that are divided by a factor proportional to presynaptic inhibitory input. It has been shown that postsynaptic shunting inhibition alone is not effective as a gain control mechanism, because the shunting will influence both EPSP amplitude and spike generation, resulting in a net subtractive effect (Holt and Koch, 1997). However, this may be different for presynaptic shunting inhibition, because only the conductance of the presynaptic membrane is altered.

In conclusion, our data provide evidence that presynaptic inhibition is a likely candidate mechanism underlying divisive operations in the nervous system. The observed gain control operates during fast sensory processing with instantaneous spike rates, an important prerequisite for many sensory modalities. In addition, we demonstrated that presynaptic inhibition enabled context specificity of gain control, because it acted only on those inputs that may need scaling.

References

Abbott LF, Varela JA, Sen K, Nelson SB (1997) Synaptic depression and cortical gain control. Science 275:220–224.

Ayaz A, Chance FS (2009) Gain modulation of neuronal responses by subtractive and divisive mechanisms of inhibition. J Neurophysiol 101:958–968.

Baca SM, Marin-Burgin A, Wagenaar DA, Kristan WB Jr (2008) Widespread inhibition proportional to excitation controls the gain of a leech behavioral circuit. Neuron 57:276–289.

Baccus SA, Meister M (2002) Fast and slow contrast adaptation in retinal circuitry. Neuron 36:909–919.

Barlow HB, Levick WR (1965) The mechanism of directionally selective units in rabbit's retina. J Physiol 178:477–504.

Benda J, Hennig RM (2008) Spike-frequency adaptation generates intensity invariance in a primary auditory interneuron. J Comput Neurosci 24:113–136.

Benda J, Herz AVM (2003) A universal model for spike-frequency adaptation. Neural Comput 15:2523–2564.

Boyan GS (1988) Presynaptic inhibition of identified wind-sensitive afferents in the cercal system of the locust. J Neurosci 8:2748–2757.

Brenner N, Bialek W, de Ruyter van Steveninck R (2000) Adaptive rescaling maximizes information transmission. Neuron 26:695–702.

Burrows M, Matheson T (1994) A presynaptic gain control mechanism among sensory neurons of a locust leg proprioceptor. J Neurosci 14:272–282.

Carandini M, Heeger DJ (1994) Summation and division by neurons in primate visual cortex. Science 264:1333–1336.

Cattaert D, El Manira A (1999) Shunting versus inactivation: Analysis of presynaptic inhibitory mechanisms in primary afferents of the crayfish. J Neurosci 19:6079–6089.

Chance FS, Abbott LF, Reyes AD (2002) Gain modulation from background synaptic input. Neuron 35:773–782.

Clarac F, Cattaert D (1996) Invertebrate presynaptic inhibition and motor control. Exp Brain Res 112:163–180.

Dean I, Harper NS, McAlpine D (2005) Neural population coding of sound level adapts to stimulus statistics. Nat Neurosci 8:1684–1689.

Gabbiani F, Krapp HG, Koch C, Laurent G (2002) Multiplicative computation in a visual neuron sensitive to looming. Nature 420:320–324.

Hardt M, Watson AH (1999) Distribution of input and output synapses on the central branches of bushcricket and cricket auditory afferent neurones: immunocytochemical evidence for GABA and glutamate in different populations of presynaptic boutons. J Comp Neurol 403:281–294.

Harris RA, O'Carroll DC, Laughlin SB (2000) Contrast gain reduction in fly motion adaptation. Neuron 28:595–606.

Hennig RM (1988) Ascending auditory interneurons in the cricket *Teleogryllus commodus* (walker): comparative physiology and direct connections with afferents. J Comp Physiol A 163:135–143.

Hildebrandt KJ, Benda J, Hennig RM (2009) The origin of adaptation in the auditory pathway of locusts is specific to cell type and function. J Neurosci 29:2626–2636.

Holt GR, Koch C (1997) Shunting inhibition does not have a divisive effect on firing rates. Neural Comput 9:1001–1013.

Imaizumi K, Pollack GS (1999) Neural coding of sound frequency by cricket auditory receptors. J Neurosci 19:1508–1516.

Imaizumi K, Pollack GS (2001) Neural representation of sound amplitude by functionally different auditory receptors in crickets. J Acoust Soc Am 109:1247–1260.

Laughlin S (1994) Matching coding, circuits, cells, and molecules to signals: general principles of retinal design in the fly's eye. Prog Retin Eye Res 13:165–196.

Libersat F, Murray JA, Hoy RR (1994) Frequency as a releaser in the courtship song of two crickets, *Gryllus bimaculatus* (de Geer) and *Teleogryllus oceanicus*: a neuroethological analysis. J Comp Physiol A 174:485–494.

Marsat G, Pollack GS (2004) Differential temporal coding of rhythmically diverse acoustic signals by a single interneuron. J Neurophysiol 92:939–948.

Marsat G, Pollack GS (2005) Effect of the temporal pattern of contralateral inhibition on sound localization cues. J Neurosci 25:6137–6144.

Marsat G, Pollack GS (2006) A behavioral role for feature detection by sensory bursts. J Neurosci 26:10542–10547.

Moiseff A, Pollack GS, Hoy RR (1978) Steering response of flying crickets to sound and ultrasound: mate attraction and predator avoidance. Proc Natl Acad Sci U S A 75:4052–4056.

Nelson M (1994) A mechanism for neuronal gain control by descending pathways. Neural Comput 6:242–254.

Nolen TG, Hoy RR (1986) Phonotaxis in flying crickets. ii. Physiological mechanisms of two-tone suppression of the high frequency avoidance steering behavior by the calling song. J Comp Physiol A 159:441–456.

Nolen TG, Hoy RR (1987) Postsynaptic inhibition mediates high-frequency selectivity in the cricket *Teleogryllus oceanicus*: implications for flight phonotaxis behavior. J Neurosci 7:2081–2096.

Olsen SR, Wilson RI (2008) Lateral presynaptic inhibition mediates gain control in an olfactory circuit. Nature 452:956–960.

Olsen SR, Bhandawat V, Wilson RI (2010) Divisive normalization in olfactory population codes. Neuron 66:287–299.

Peña JL, Konishi M (2001) Auditory spatial receptive fields created by multiplication. Science 292:249–252.

Prescott SA, De Koninck Y (2003) Gain control of firing rate by shunting inhibition: Roles of synaptic noise and dendritic saturation. Proc Natl Acad Sci U S A 100:2076–2081.

Root CM, Masuyama K, Green DS, Enell LE, Nässel DR, Lee CH, Wang JW (2008) A presynaptic gain control mechanism fine-tunes olfactory behavior. Neuron 59:311–321.

Rothman JS, Cathala L, Steuber V, Silver RA (2009) Synaptic depression enables neuronal gain control. Nature 457:1015–1018.

Rudomin P (2009) In search of lost presynaptic inhibition. Exp Brain Res 196:139–151.

Laughlin SB (1989) The role of sensory adaptation in the retina. J Exp Biol 146:39–62.

Salinas E, Thier P (2000) Gain modulation a major computational principle of the central nervous system. Neuron 27:15–21.

Selverston AI, Kleindienst HU, Huber F (1985) Synaptic connectivity between cricket auditory interneurons as studied by selective photoinactivation. J Neurosci 5:1283–1292.

Shapley R, Enroth-Cugell C (1984) Visual adaptation and retinal gain controls. Prog Retin Res 3:263–346.

Silver RA (2010) Neural arithmetics. Nat Rev Neurosci 11:474–489.

Todd BS, Andrews DC (1999) The identification of peaks in physiological signals. Comput Biomed Res 32:322–335.

VanLeeuwen M, Fahrenfort I, Sjoerdsma T, Numan R, Kamermans M (2009) Lateral gain control in the outer retina leads to potentiation of center responses of retinal neurons. J Neurosci 29:6358–6366.

Watson AH, Hardt M (1996) Distribution of synapses on two local auditory interneurones, ON1 and ON2, in the prothoracic ganglion of the cricket: relationships with GABA-immunoreactive neurones. Cell Tissue Res 283:231–246.

Wen B, Wang GI, Dean I, Delgutte B (2009) Dynamic range adaptation to sound level statistics in the auditory nerve. J Neurosci 29: 13797–13808.

Wimmer K, Hildebrandt KJ, Hennig RM, Obermayer K (2008) Adaptation and selective information transmission in the cricket auditory neuron an2. PLoS Comput Biol 4:e1000182.

Wohlers DW, Huber F (1978) Intracellular recording and staining of cricket auditory interneurons (*Gryllus campestris* L., *Gryllus bimaculatus* DeGeer). J Comp Physiol A 127:11–28.